Chinese Chemical Letters 34 (2023) 108492

Contents lists available at ScienceDirect

Chinese Chemical Letters

journal homepage: www.elsevier.com/locate/cclet

Distorted aryl homochirality controlled by β-sheet folding

Yunying Xu, Aiyou Hao*, Pengyao Xing*

School of Chemistry and Chemical Engineering, Shandong University, Ji'nan 250100, China

ARTICLE INFO

Article history:
Received 5 January 2023
Revised 7 April 2023
Accepted 20 April 2023
Available online 23 April 2023

Keywords:
Distorted chirality
Folding
Solvent strategy
Chiroptical activity

ABSTRACT

Distortion of planar aromatics occurs in the fused rings conjugated with bulky substituents, which generates racemic enantiomers with high transformation energy barriers. However, direct synthesis of homochiral distorted aryl compounds is a very challenging task. Here, we presented a molecular folding strategy to control distorted aryl homochirality. Amino acids and their derivatives conjugated on the polycyclic aromatic hydrocarbons including benzenes, naphthalenes and triphenylenes, which formed parallel β-sheet arrays through intramolecular hydrogen bonds. The folding behavior enabled distorted or twisted geometry of aromatics, of which the handedness was associated with the absolute chirality of amino acids. X-ray crystallography, theoretical calculations and circular dichroism spectroscopy verified the distorted homochirality in the solid and solution phase. The relatively small rotational barrier between the enantiomers made the molecule sensitive to the environment and thus realized the solvent-controlled chiral inversion. The β-sheet folding strategy can be widely used in polycyclic aromatic hydrocarbons with various functions, which provided a promising strategy to control inherent chirality of aromatics with adaptive chiroptical responses.

Inherent aryl chirality such as axial, planar and helical chirality are of vital importance in the asymmetrical synthesis, chiral separation, sensing and chiroptical applications [1–4]. Binaphthyl [5], cyclophane [6], and helicene [7] are three typical chiral aromatics with inherent chirality, which show great potentials in the design of catalyst ligands and circularly polarized luminescence (CPL) [8–10]. Distorted or twisted chirality, as an atypical chirality, refers to the planar aromatics with specific distorted geometries compelled by the adjacent substituents with bulky steric hindrance [11]. For instance, two adamantane groups conjugated on the 1,8-position of naphthalene would greatly twist the aromatic plane (Scheme 1a) [12]. Bay substitution of perylene bisimides (PBIs) introduced steric congestion, leading to the twisted aromatic core [13]. Distorted π-backbones feature tunable structural rigidity, showing diverse photophysical and chiral properties, which express potential applications in the organic electronics and spintronics [14]. To gain enantiomeric pure distorted compound, high-performance liquid chromatography (HPLC) separation was often required due to the relatively large transformation energy barrier as well as the poor-controlled chirality during synthesis [15,16].

Molecular folding driven by intramolecular noncovalent forces such as hydrogen bonds or π-stacking would efficiently transfer point chirality from substituents to aromatics [17–20]. By this strategy, axial and propeller chirality of aromatics have been realized in hydrogen bonded folded structures [21,22]. However, the control over distorted homochirality using folding is unprecedented. It is envisioned that the bay substitution of amino acid derivatives would enable hydrogen bonded β-sheet folding, which may arouse plane distortion and achieve chirality transfer [23,24]. In this work, we reported a folding strategy to control the distorted aryl chirality and dynamic control over chirality was realized by switching solvents, which ascribed to the small energy barrier between enantiomeric conformations. This strategy produced enantiopure distorted polycyclic aromatic hydrocarbons without further HPLC separation, of which chirality was controlled by the amino acids. The π-conjugated core showed wide structural scope including benzene, naphthalene and triphenylbenzene (Scheme 1). Due to the weak nature of hydrogen bonds, the specific molecule showed solvent adaptivity that N-Ala-displayed a chirality inversion in tetrahydrofuran (THF) and *N,N*-dimethyl formamide (DMF).

The formation of distorted chirality was verified based on X-ray crystal structure, circular dichroism spectra and density functional theory (DFT) calculations. The folded structures perform as building units undergoing bottom-up self-assembly into nanoscale helical structures, and multi-level chiral evolution can be realized. This work revealed the key role of amino acid folding to control the distortion of polycyclic aromatic hydrocarbons and provided a promising strategy to regulate the chiral property of intrinsic aryl

* Corresponding authors.
E-mail addresses: haoay@sdu.edu.cn (A. Hao), xingpengyao@sdu.edu.cn (P. Xing).

https://doi.org/10.1016/j.cclet.2023.108492
1001-8417/

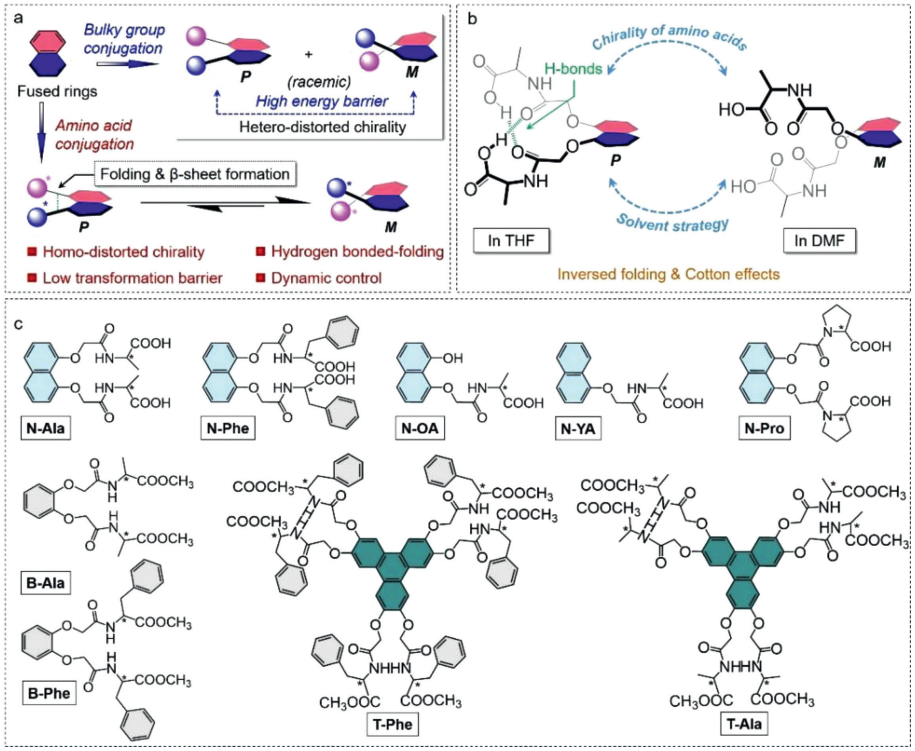

Scheme 1. (a) Schematic presentation of the naphthalene distortion induced by steric hindrance effects and side arms strategy of substituents, as well as our strategy to anchor chiral entities to realize fixed twisted conformation and the kinetic control. (b) Conformational variation in different solvents of N-Ala. (c) Molecular structures of different amino acid derivatives synthesized in this work.

groups, which is of great significance for the design and development of CPL and organic electronics.

To verify the chiral conformation in the solution phase, we carried out circular dichroism (CD) spectroscopy. Solvent polarity has potential influence on the chiral structures and intramolecular weak interactions. In THF, 1,4-dioxane (DIOX) and methanol (MeOH), N-^{L}Ala afforded complicated Cotton effects centered at around 300 nm with positive and negative peaks at 330 nm and 290 nm, respectively. However, a chirality inversion phenomenon was observed in DMF and dimethyl sulfoxide (DMSO), which showed opposite Cotton effects, compared to that of THF, MeOH and DIOX. The D-enantiomer gave to the corresponding mirror CD spectrum (Figs. 1a and b, Fig. S21 in Supporting information). The Cotton effect was caused by intramolecular transfer from chiral centers to the distorted aryl regions. In addition, in THF and DMF, CD spectra of N-Phe-failed to reverse, and a mirror CD curve was given for the D-enantiomer. CD signals at around 290 nm (positive) and 330 nm (negative) for N-^{L}Phe and the signal was five times stronger than that of N-Ala-due to the steric hindrance effects (Fig. 1c and Fig. S22 in Supporting information). As shown in Fig. 1d, B-^{L}Phe and B-^{D}Phe showed positive and negative Cotton effects respectively at 275 nm in THF, which is assigned to the region of the benzene ring. However, B-^{L}Ala showed silent CD signals in solvents, which indicated the steric hindrance effect was significant to anchor the molecular geometry and facilitated the transfer of chirality (Fig. S23 in Supporting information). Compared with N-Ala, no signal reversal was found in T-Ala, which displayed Cotton effects centered at around 290 nm with positive and negative peaks at 300 nm and 263 nm, respectively. The D-enantiomer gave to the corresponding mirror CD spectrum in THF (Fig. 1e). T-^{L}Ala with six chiral arms, may afford rich intramolecular hydrogen bond networks and multiple CH···π bonds, which shall enhance the transformation energy barrier. T-^{L}Phe displayed negative Cotton effect at around 313 nm and positive Cotton effect at about

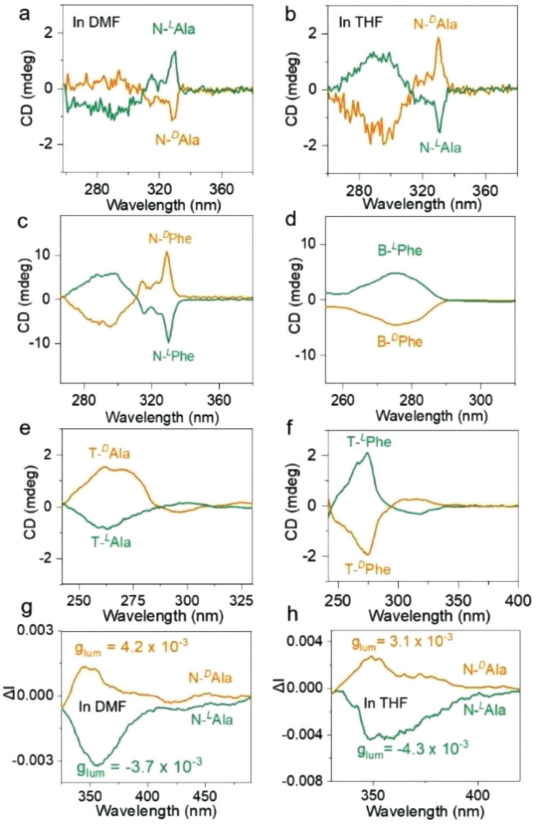

Fig. 1. Chiroptical activities. (a, b) CD spectra of N-Ala (1 mmol/L in DMF and THF, respectively). (c) CD spectra of N-Phe-in THF (1 mmol/L). (d) CD spectra of B-Phe-in THF (4 mmol/L). (e, f) CD spectra of T-Ala-in THF and T-Phe-in DIOX (0.08 mmol/L), respectively. (g, h) CPL spectra of N-Ala-immobilized in polymethylmethacrylate (PMMA) matrices. Solvents were DMF and THF, respectively (λ_{ex} = 300 nm).

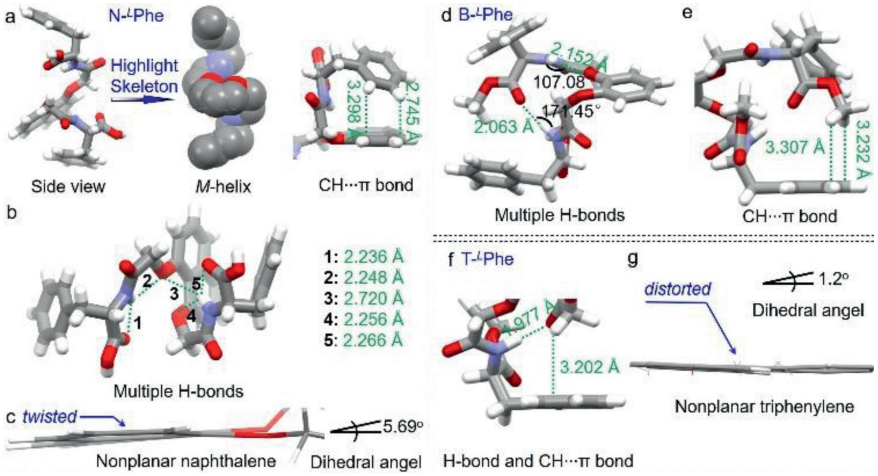

Fig. 2. (a) X-ray structure of N-^{L}Phe. (b) Intramolecular hydrogen bonds of N-^{L}Phe. (c) Distortion angle of the nonplanar naphthalene. (d, e) DFT optimized geometries of B-^{L}Phe and (f, g) DFT optimized T-^{L}Phe geometry at the theory level of B3LYP/6–311G(d).

275 nm, and T-^{D}Phe had the corresponding mirror CD spectrum in DIOX. N-^{L}OA, N-^{L}Pro and N-YA showed silent CD signals in solvents (Figs. S24-S26 in Supporting information). Based on the special structure of molecular, N-^{L}OA and N-YA with one chiral arm and N-^{L}Pro molecules cannot have the conditions to form intramolecular hydrogen bonds, so they failed to form the β-sheet folding. Chirality is not transferred to the naphthyl group, which is the expected CD silence.

To further verify the assumed intramolecular folding by hydrogen bonds, variable temperature (VT) CD spectra were recorded. Increasing temperature from 293 K to 353 K the Cotton effect of N-^{L}Ala slightly decrease in DIOX and DMSO (Fig. S27 in Supporting information). VT nuclear magnetic resonance (NMR) spectra from 303 K to 333 K in deuterated DMSO were studied as well (Fig. S28 in Supporting information). With increasing temperature from 303 K to 333 K, amide proton shifted to higher fields with a shift of 0.12 ppm. It suggested that the amide proton-involved hydrogen bonds were disassociated upon heating, verifying the hydrogen bonded folding structure. In order to further explore the effect of solvent on chiroptical activities, we evaluated the CPL spectra of N-Ala. CPL has great potential for application in optical sensors and optoelectronic devices. In DMF, N-^{L}Ala and N-^{D}Ala features left-handed and right-handed CPL with a maximum peak at 355 nm for L- and D-enantiomer respectively (Figs. 1g and h), with g_{lum} at 10^{-3} order of magnitude at their extremum emission wavelengths. When the solvent was switched to THF, N-Ala-showed identical CPL signal at the same wavelength, which disagreed with the CD inversion as shown in Figs. 1a and b. Due to the solvent was evaporated to form a solid film, chirality at photoexcited state cannot displayed inversion in the absence of solvent.

To further understand the effect of folding behavior on the chiral geometry, single crystals were cultivated. N-^{L}Phe and N-^{L}OA successfully crystallized in the acetone/decane mixtures *via* liquid phase diffusion. In the crystal structure, the molecular skeleton of N-^{L}Phe folded into an *M*-helix structure (Fig. 2a). This helical structure was reminiscent of α-helical structure directed by two chiral molecular arms. *M*-handed helix originated from the absolute chirality of amino acid, which twisted naphthalene plane to compensate the formation of the helical turn and the helical structure was stabilized by several noncovalent interactions, including multiple H-bonds and CH···π. Distances of CH···π bonds between benzene and naphthalene were determined as 2.745 and 3.298 Å, respectively (Fig. 2a). Multiple intramolecular hydrogen bonds further anchor the spiral conformation (Fig. 2b). The presence of amides and carboxylic acids induced the formation of multiple intramolecular hydrogen bonds. Distances were determined as 2.236, 2.248, 2.945, 2.720, 2.256 and 2.266 Å, respectively. Multiple intramolecular hydrogen bonds further stabilized the structure and properties of molecules. Due to the folding and steric hindrance effect, the naphthalene plane was deformed under the control of two chiral arms with a dihedral angle of 5.69° (Fig. 2c). The twisted naphthalene contributed to the active chiroptical properties measured in solution. The DFT optimized structure of B-^{L}Phe and T-^{L}Phe showed a closed geometry with intramolecular multiple H-bonded networks and CH···π bonds. As shown in Fig. 2d, the distance of the hydrogen bond was 2.063 Å and 2.152 Å, with ∠N–H···O angle of 107.05° and 171.45°, respectively. In Fig. 2e, the CH···π distances were determined as 3.307 Å and 3.232 Å respectively. In addition, some of the molecular fragments of T-^{L}Phe were shown in Fig. 2f, the hydrogen bond with a distance of 1.977 Å was found. As shown in Fig. 2g, the triphenylbenzene region of T-^{L}Phe represented slightly distorted, forming a nonplanar structure with the dihedral angle of 1.2° [25–27].

To explore the molecular folding structure of N-^{L}Ala and T-^{L}Ala, geometry optimizations were carried out at the B3LYP/6–311G(d) level of theory. In Fig. 3a, multiple intramolecular hydrogen bonds were induced between carboxylic acids, amide and oxygen atoms. Distances were determined as 1.752, 1.927, 2.105 and 2.168 Å, respectively. The relative orientation of alanine constitutes in a parallel β-sheet array. The dihedral angle of nonplanar naphthalene was determined as 9.5° The twisted orientation was identical to that of N-^{L}Ala, which in good agreement with their identical shape of Cotton effects. It means the crucial effect of twisted naphthalene on the emerged Cotton effects and CPL activities. Compared to N-^{L}Phe, N-^{L}Ala lacks the steric hindrance effect as well as CH···π bond, resulting in the relatively weak molecular rigidity and weak Cotton effects. In the crystal structure of N-^{L}OA (Fig. 3b), the hydrogen bond with a distance of 2.143 Å was found between the amide proton and hydroxyl group. Compared to N-^{L}Phe and N-^{L}Ala, the mono-intramolecular hydrogen bond of N-^{L}OA is possibly hardly to anchor the chiral conformation, resulting in the silent chiroptical activity. The adopted space group ($P2_12_12_1$) of N-^{L}OA is chiral, of which crystal lattice comprises of a hydrogen bonded dimer *via* complementary hydrogen bonds with the distance of 1.869 Å, with a ∠X-H···O angle of 163.13°. The intramolecular interactions induced a three-dimensional structure and the hydrogen bond possessed good linearity between hydroxyl groups and carboxylic acids. Naphthalene moieties were highlighted by CPK mode with red and blue, which showed that hydrogen bonds induced

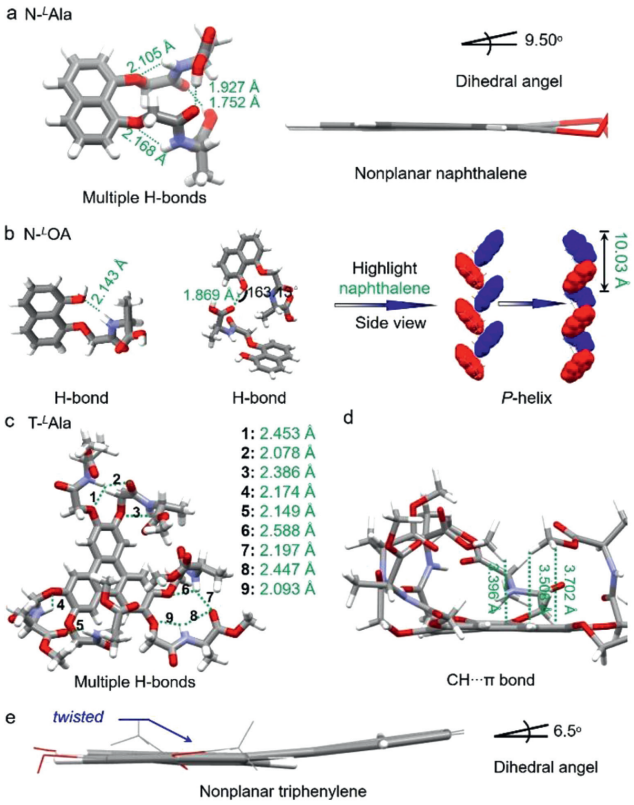

Fig. 3. (a) DFT optimized N-^{L}Ala at the B3LYP/6–311G(d) level of theory. (b) X-ray structure of N-^{L}OA. Naphthalene moieties were highlighted in CPK mode to show the supramolecular helical structure. (c-e) DFT optimized geometry of T-^{L}Ala at the B3LYP/6–311G(d) level of theory.

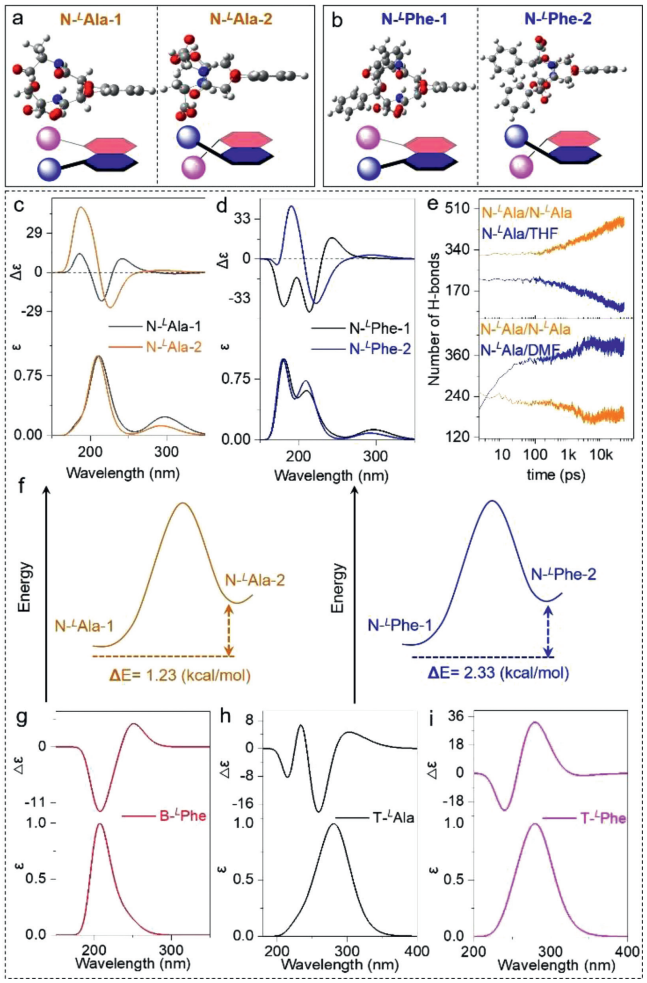

Fig. 4. (a, b) Optimized structures with different arm-orientation of N-^{L}Ala and N-^{L}Phe. (c, d) Calculated ECD spectra between two different conformations. (e) The number of hydrogen bonds in THF and DMF, respectively. (f) Calculated energy barriers of N-^{L}Ala and N-^{L}Phe. (g-i) Calculated ECD spectra of B-^{L}Phe, T-^{L}Ala and T-^{L}Phe at the B3LYP/6–311G(d) level.

P-handed helical packing with respect to naphthalene moieties under the side view, where helical pitch was determined as 10.03 Å. For hydrogen bonds, the ∠X-H···O angle was usually linear (around 180°), and deviations from this angle usually reduced the strength of the hydrogen bond. As shown in Fig. 3c, T-^{L}Ala linked to six chiral arms, which exhibited a multiple hydrogen bonds network and CH···π. Distances of multiple H-bonds were determined as 2.078, 2.093, 2.149 and 2.174 Å. The molecular arms were pally connected by hydrogen bonds between amides. The distance of CH···π were 3.396, 3.508 and 3.702 Å (Fig. 3d). In Fig. 3e, the aryl region of T-^{L}Ala represented a twisted nonplanar structure with a dihedral angle of around 6.5°, which indicated the side arm strategy and molecular folding was a favorable way to control the distortion of aryl groups and transfer of chirality.

To explore the correlation between molecular conformation and chiroptical properties, electronic circular dichroism (ECD) spectra were calculated *via* time-dependent density functional theory (TD-DFT). Spartan 14 software was used to search and calculate molecular conformations after optimization of Merck molecular force field. All configurations with values above 0 are derived from Energy and Boltzmann distribution. TD-DFT at the B3LYP/6–311G(d) level was used to optimize and calculate ECD spectra until right conformations were found, which were consistent with experimental results. For both N-^{L}Ala and N-^{L}Phe, two opposite conformations were built and optimized with either "front-up/back-down" and "front-down/back-up" orientation (Figs. 4a and b). The first Cotton effect band for N-^{L}Ala-1 and N-^{L}Ala-2 was positive and negative, respectively, indicating the orientation of two arms determined the Cotton effect (Fig. 4c), which means variation of solvent aroused switchable arms movement between two conformations. Similar results were found in the ECD spectra of N-^{L}Phe (Fig. 4d). In order to further explore the folding parameters in different solvents, molecular dynamics simulations of N-^{L}Ala in THF and DMF were carried out. The molecular geometry model of N-^{L}Ala was built, and structural optimization was carried out at the B3LYP/6–311G(d) level. No virtual frequency was present during optimization to ensure the minimum energy structure. Results were fitted with restrained electrostatic potential charge by Antechamber program. The solvent models of THF and DMF were obtained by the same method. After calculation, the number of hydrogen bonds was counted. As shown in Fig. 4e, in THF, the number of hydrogen bonds formed between N-^{L}Ala was about four times higher than that between N-^{L}Ala and THF molecules. However, in DMF, a different propensity was observed. The number of hydrogen bonds formed between N-^{L}Ala and DMF molecules was about two times higher than that between N-^{L}Ala molecules. In THF, N-^{L}Ala molecules tended to form hydrogen bonds with conspecific molecules. However, in DMF, the hydrogen bond between N-^{L}Ala was disassociated by DMF molecules, resulting in the solvation. It means that DMF solvation destructed the intramolecular folding behaviors, which provided an opportunity for conformational transformations and helicity inversion. The geometry optimization of complexes with different conformations were deposited to DFT calculation at the theory level of B3LYP/6–311G(d). The Electronic Energy and Thermal Free Energy Correction were

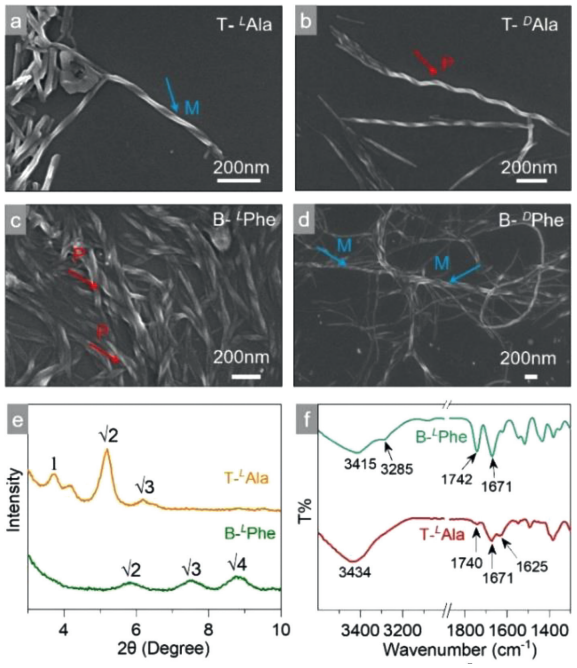

Fig. 5. SEM images of self-assembly systems: (a) T-^{L}Ala, (b) T-^{D}Ala, (c) B-^{L}Phe, (d) B-^{D}Phe (concentrations of each component were fixed at 1 mmol/L). (e) XRD spectra of T-^{L}Ala and B-^{L}Phe assemblies. (f) FT-IR spectra of T-^{L}Ala and B-^{L}Phe assemblies.

obtained. Energy barriers were calculated in vacuum. Energy diagrams (Fig. 4f) showed energy barriers between two conformations of N-^{L}Ala and N-^{L}Phe, which were 1.23 kcal/mol and 2.33 kcal/mol, respectively. The result revealed the low energy barrier for the solvent-induced signal reversal behaviors of N-^{L}Ala. The ECD spectra with the lowest-energy conformer were simulated. In Fig. 4g, B-^{L}Phe exhibited positive Cotton effect bands at 250 nm. As shown in Fig. 4h, T-^{L}Ala exhibited positive and negative Cotton effect bands at 300 nm and 260 nm, respectively. T-^{L}Phe exhibited positive and negative Cotton effect bands at 280 nm and 240 nm, respectively (Fig. 4i). The ECD spectra were in good agreement with the experimental results, which reflected the folded structures in solutions.

These N-terminal aromatic amino acids are candidates for bottom-up self-assemblies, which could realize chirality transmit to macroscopic scale. Scanning electron microscopy (SEM) and transmission electron microscopy (TEM) were used to probe the supramolecular chirality found in self-assemblies. For the self-assembly of T-^{L}Ala and T-^{D}Ala, twisted nanofibers were observed in aqueous media. Enlarged images indicate that T-^{L}Ala self-assemblies showed homochiral *M*-handedness (Fig. 5a). As shown in Fig. 5b, the T-^{D}Ala self-assemblies are with the opposite homochirality of P-handedness. Similarly, both left-handed and right-handed chiral nanofibers also showed chiral structures for B-^{L}Phe (Fig. 5c) and B-^{D}Phe (Fig. 5d), indicating the enantiomer-directed supramolecular chirality. Based on the morphological observation, B-Phe-self-assembled into chiral nanofibers, while N-Phe-formed two-dimensional thin-film structures (Fig. S29 in Supporting information) and short rod nanostructures appeared in the T-Phe (Fig. S30 in Supporting information). A variety of self-assembled nanostructures were induced by different aryl groups and chiral arms. The structural characteristics of different conjugated groups and the influence of the steric hindrance of chiral molecular arms lead to the change of the stacking mode of building units, which greatly affects the molecular assembly mode and leads to the change of supramolecular assembly morphology [28–33]. This correlation could provide an intuitive understanding of the structural basis of chiral optical properties. X-ray diffraction (XRD) patterns were investigated to reveal the varied molecular arrangement of the assemblies. Self-assembled aggregates were obtained by the high-speed centrifugation, then coated on glass sheets and dried at room temperature. In Fig. 5e, several diffraction peaks of B-^{L}Phe at small angle region are found, with D-spacing ratio of $\sqrt{2}$: $\sqrt{3}$: $\sqrt{4}$. Such a ratio corresponds to the orthogonal packing in the self-assembled helices. In comparison, T-^{L}Ala adopts a hexagonal packed array with a large primary D-spacing value of 2.40 nm due to the relatively large molecular length and C3 symmetry. Fourier transform infrared spectroscopy (FT-IR) was showed in Fig. 5f. The bands at 3434 and 3415 cm^{-1} from T-^{L}Ala and B-^{L}Phe were assigned to the N–H stretching vibration bands. However, a shifted band at 3285 cm^{-1} was found in B-^{L}Phe, which corresponded to arrays of the intermolecular hydrogen bonded. This assumption was further verified by an appearance of the amide-I band at 1742 cm^{-1}.

In conclusion, we reported a molecular folding approach to induce twisted aryl chirality, which could also be tuned by solvent strategy. Amino acid derivatives were covalently conjugated on polycyclic aromatic hydrocarbons, which formed hydrogen bonded β-sheet structures. The chiral transfer of amino acids was facilitated by the folding strategy and the distortion of a polycyclic aromatic plane that forced by hydrogen bonding, CH···π interactions and steric hindrance effects of substituents. The amino acid substitution and β-sheet structure played a key role in the emergence, transfer and amplification of chirality, which was further confirmed by X-ray structure, CD, CPL and DFT calculations. The experimental and theoretical studies described the design and preparation of nine chiral aryl compounds, and folding behaviors and side arms strategy were used to induce twisted aryl chirality and influenced chiroptical activities, which would promote the design of new types of chiral molecular arms for supramolecular chiral functional materials and broaden the chiral scope of application of non-planar aryl materials.

Declaration of competing interest

The authors declare that they have no known competing financial interests or personal relationships that could have appeared to influence the work reported in this paper.

Acknowledgments

This work is also supported by the National Natural Science Foundation of China (Nos. 21901145, 22171165). We also acknowledge the financial support from Youth cross-scientific innovation group of Shandong University (No. 2020QNQT003).

Supplementary materials

Supplementary material associated with this article can be found, in the online version, at doi:10.1016/j.cclet.2023.108492.

References

[1] G. Bringmann, T. Gulder, T. Gulder, M. Breuning, Chem. Rev. 111 (2011) 563–639.
[2] C. Shi, H. Li, X. Shi, L. Zhao, H. Qiu, Chin. Chem. Lett. 33 (2022) 3613–3622.
[3] D. Zheng, C. Yu, L. Zheng, H. Jiang, Chin. Chem. Lett. 31 (2020) 673–676.
[4] S. Sakamoto, T. Taniguchi, Y. Sakata, et al., Angew. Chem. Int. Ed. 133 (2021) 22375–22380.
[5] K. Takaishi, M. Yasui, T. Ema, J. Am. Chem. Soc. 140 (2018) 5334–5338.
[6] Y. Sagara, H. Traeger, J. Li, et al., J. Am. Chem. Soc. 143 (2021) 5519–5525.
[7] Y. Wang, Z. Yin, Y. Zhu, et al., Angew. Chem. Int. Ed. 131 (2019) 597–601.
[8] Z. Sun, J. Liu, D. Yuan, et al., Angew. Chem. Int. Ed. 58 (2019) 4840–4846.
[9] S. Jiang, S. Zhou, Y. Chen, H. Guo, F. Yang, Chin. Chem. Lett. 33 (2022) 2442–2446.
[10] Z. Yu, H. Bisoyi, X. Chen, et al., Angew. Chem. Int. Ed. 61 (2022) e202200466.
[11] A. Ishii, A. Shiotari, Y. Sugimoto, Chem. Sci. 12 (2021) 13301–13306.

[12] K. Yamamoto, N. Oyamada, S. Xia, et al., J. Am. Chem. Soc. 135 (2013) 16526–16532.
[13] S. Penty, M. Zwijnenburg, G. Orton, et al., J. Am. Chem. Soc. 144 (2022) 12290–12298.
[14] S. Shimizu, S. Nakano, A. Kojima, N. Kobayashi, Angew. Chem. Int. Ed. 53 (2014) 2408–2412.
[15] Q. Wang, A. Pietropaolo, M. Fortino, et al., Chirality 34 (2022) 317–324.
[16] W. Zhang, R. Ekomo, C. Roussel, et al., Chirality 30 (2018) 498–508.
[17] D. Zhang, W. Wang, Z. Li, Chem. Rec. 15 (2015) 233–251.
[18] L. Chen, Y. Wang, B. He, et al., Angew. Chem. Int. Ed. 54 (2015) 4231–4235.
[19] S. Mathew, L. Crandall, C. Ziegler, C. Hartley, J. Am. Chem. Soc. 136 (2014) 16666–16675.
[20] Y. Xiong, C. Huang, H. Liu, et al., Chin. Chem. Lett. 32 (2021) 3522–3525.
[21] B. Liu, A. Hao, P. Xing, J. Phys. Chem. Lett. 12 (2021) 6190–6196.
[22] J. Zhao, A. Hao, P. Xing, ACS Nano 16 (2022) 4551–4559.
[23] S. Reddy, S. Pal, S. Ghosh, E. Prabhakaran, ChemBioChem 22 (2021) 2111–2115.
[24] J. Ross, P. Knipe, S. Thompson, A. Hamilton, Chem. Eur. J. 21 (2015) 13518–13521.
[25] J. Li, A. Terec, Y. Wang, et al., J. Am. Chem. Soc. 139 (2017) 3089–3094.
[26] Y. Peng, L. Li, C. Zhu, et al., J. Am. Chem. Soc. 142 (2020) 13162–13169.
[27] Z. Gong, X. Zhu, Z. Zhou, et al., Sci. China Chem. 64 (2021) 2060–2104.
[28] X. Chen, W. Feng, H. Bisoyi, et al., Nat. Commun. 13 (2022) 3216.
[29] Y. Xu, A. Hao, P. Xing, Angew. Chem. Int. Ed. 61 (2022) e202113786.
[30] X. Chen, X. Hou, H. Bisoyi, et al., Nat. Commun. 12 (2021) 4993.
[31] S. Liao, X. Sun, Y. Tang, Acc. Chem. Res. 47 (2014) 2260–2272.
[32] Z. Wang, A. Hao, P. Xing, Chin. Chem. Lett. 32 (2021) 1390–1396.
[33] X. Liu, K. Wang, M. Externbrink, et al., Chin. Chem. Lett. 31 (2020) 1239–1242.